Simulation of Heat Loss in CZTSSe Thin Film Solar Cells: A Coupled Optical-Electrical-Thermal Modeling

Soma Zandi
independent researcher
Mohsen Jamshidi Seresht
independent researcher
NIMA E. Gorji (nima.s.gorji@gmail.com)
Dublin City University

Research Article

Keywords: Thin film, CZTSSe, Heat generation, Heat dissipation, 3D simulation, Coupled modeling, Solar cells

Posted Date: February 26th, 2021

DOI: https://doi.org/10.21203/rs.3.rs-266986/v1

Simulation of Heat Loss in CZTSSe Thin Film Solar Cells: A Coupled Optical-Electrical-Thermal Modeling

Soma Zandi[a], Mohsen Jamshidi Seresht[a], Nima E. Gorji[b,*]

[a] *Independent Researcher*
[b] *School of Physics, Dublin City University, Ireland*

Abstract

A coupled optical-electrical-thermal modeling has been developed to investigate the heat generation in CZTSSe solar cells via Thermalization, Joule heat, Peltier heat, Surface Recombination heat, and non-radiative recombination heat and also the heat dissipation via convective and radiative cooling. These were calculated and displayed in 2D and 3D maps either at zero bias or open-circuit voltage (V_{oc}) conditions. At V=0, the heat is generated mainly at the junction of CZTSSe/CdS where the thermalization and Joule heats are dominantly higher compared to non-radiative (SRH and Auger) recombination heat. However, at V=V_{oc}, the nan-radiative recombination heat becomes comparatively higher than the Joule heating whereas the thermalization remains highest as before. Apart from the bulk heating factors, we also studied the surface recombination and Peltier heat generation. The surface recombination heat is higher at V=V_{oc} compared to at V=0 while the Peltier heat is zero at V=V_{oc} which can be explained by looking at the energy band diagrams at these voltages. The total heat generation does not change much across the cell thickness ($<5\times10^9$ W/m^3) as the cell is quite thin. Nevertheless, the individual impact of every heat generation factor on power-density and current-voltage characteristics of the cell reveals that the thermalization, Joule, and non-radiative recombination heats reduce the open-circuit voltage of the cell from 0.54 V to 0.49 V (ΔV= 0.047 V) while the Peltier and surface recombination heat is less effective. The temperature of the cell shows a small distribution across the cell (0.01 K). However, the temperature of the initial study at 293 K increases to 315-320 K for the coupled study. At this increased temperature, the short current-density doesn't change but the fill factor decreases from 73.8% to 71.8% and, therefore, the energy conversion efficiency of the cell falls by 11.11% (from initial 12.78% to 11.36%). All the total heat dissipation, convective, and radiation cooling follow a similar trend to the total heat generation but convective cooling is the dominant component of dissipation.

Keywords: Thin film, CZTSSe, Heat generation, Heat dissipation, 3D simulation, Coupled modeling, Solar cells.

1. Introduction

Although solar cells are thermodynamic devices, the heat generation and dissipation mechanisms have been rarely investigated in these devices especially through modeling or simulation analysis. The lifetime aging analysis (damp-heat experiments) suggest a significant impact of the heat generation on performance stability of solar cells [1, 2]. Heat generation/dissipation becomes more important for light management designs and light concentration photovoltaics where the thermodynamic of the cell can dramatically limit the device operation and stability through self-healing (surface/bulk non-radiative recombination) and light-absorption heating (thermalization) [3]. Therefore, analyzing the heat generation factors and their impact on device characteristics is essential to explore a way to keep a balance between the heat generation and dissipation in the cell for operation stability and physical quality of the cells. Previous simulation analysis demonstrated that the thermodynamic of the solar cells are firmly coupled to optical and electrical mechanisms [4, 5]. Through coupled optical-electrical-thermal (OET) simulations, Shang and Li have calculated the impact of five heating generation factors on the current-voltage and power-voltage of GaAs solar cells and showed that the Thermalization and Joule heat (158 W/m^2 and 121 W/m^2) are the main heating components compared to surface recombination heat, Peltier heat and non-radiative recombination (Shockley-Read-Hall, SRH and Auger recombination) heat (10-30 W/m^2) [6]. In our previous studies, we have presented our coupled simulation analysis of heat distribution across a CZTSSe solar cell contacted with an rGO electrode [7]. The individual impact of these heating factors was not considered separately but only the total heat generated in the cell was investigated. In this paper, we investigated the impact of every heat generation component on the current-voltage characteristics of CZTSSe thin-film solar cells using FEM modeling and a 3D simulation analy-

* *Email address:* Corresponding author: nima.gorji@dcu.ie (Nima E. Gorji)

sis. Five heat generation factors were identified for a typical $Cu_2ZnSn_4S_xSe_{4-x}$ (CZTSSe) solar cell and the heat generation was simulated for the initial and coupled models. We coupled three optical, electrical (semiconductor) and thermal modules and investigated the heat distribution, current-voltage characteristics dependency on temperature, and the voltage-dependency of heat generation rate at zero voltage or V=V_{oc} conditions. The heat dissipation through convective and radiative cooling has been also studied to uncover the balance required for the stable operation of the cell from a thermodynamic point of view.

2. Structure, Mesh & Simulation Procedure

We adapted the structure of CZTSSe solar cell that was developed by IBM with a record efficiency report of 12.6% [8]. Recently, we presented a 3D FEM and coupled simulation study on the same thin film CZTSSe kesterite structure (Mo/Mo(S,Se)$_2$/CZTSSe/CdS/ZnO/ITO/air) for the optical generation, electric field distribution, recombination rate, current-voltage characteristics, thermal and heat distribution maps [7]. The same structure (Fig. 1) will be used here to study the heat generation factors and their impact on device characteristics. We added a block of Air on top of the structure where the sunlight of AM1.5G (1 sun) illuminates with 100 mW/cm^2 for a range of 300-1000 nm solar spectrum at a normal incident angle. The materials properties, optical, electrical, and thermal constants are added from the respective references [9, 10, 11] as presented in Table 1 of our recent publication in Ref. [7]. Besides the mentioned parameters, Auger and direct recombination parameters have also been included in the simulations as the other recombination heating mechanisms, while SRH recombination is the dominant recombination process in the structure and has a significant heat generation rate. A free quad mesh type was applied at the plane boundary perpendicular to the cell thickness (vertical axis). This mesh was then swept across the cell thickness direction with different sizes, ranging from 2.7 nm to 72.7 nm. In this case, a total of 6096 hexahedral mesh elements were made in the structure. We set the initial temperature of the cell equal to environment temperature at room temperature (T_{env}= 293 K).The optical model was solved to calculate the optical photo-generation rate across the cell which has been used as an input for the electrical model. Then, the electrical model was calculated to produce the current-voltage characteristics and the heat-induced energy losses caused by semiconductor mechanisms in the solar cells. The latter was used as a coupling connected to the thermal model. Five different heat generation factors were included in the thermal model as shown in Fig. 2, each of these mechanisms will be discussed in more detail in the following sections. It is assumed (and set) that the heat is dissipated to the air environment through radiation and convection from the top and bottom surfaces only. There are no heat fluxes

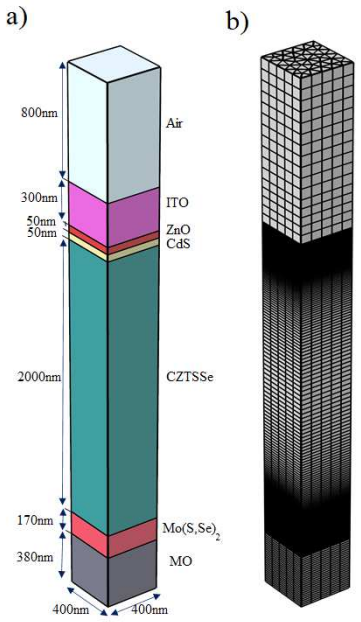

Figure 1: a)The 3D structure of the proposed CZTSSe/CdS thin film solar cell adopted from IBM's record cell efficiency [8], b) the meshed structure

from the side boundaries of the cell. Hence, thermal insulation boundary conditions were applied for these walls in the heat transfer module. The IBM record efficiency cell has been designed for the simulation to make the model closer to reality. The top-most layer is modeled as air, extending up to 800 nm in height. The input power of the plane wave (300-1000 nm) was AM1.5G with a normal incident angle only. This layer is followed by a 300 nm ITO layer. ZnO and CdS layers with 50nm thickness each have been inserted between the ITO and CZTSSe layers where the PN-junction forms and the electric-field can collect the carriers via drift component. The thickness of the CZTSSe layer is 2000 nm on MO(S,Se)$_2$ layer (170 nm) followed by the last layer Mo with 380 nm thickness at the bottom. The overall dimension of the cell is 400 nm × 400 nm × 3750 nm. The cell is assumed to be initially operating at room temperature where we calculated the heat components (*Initial study*). The semiconductor module is completely coupled to the heat transfer module to run the *coupled study*. The heat generation factors calculated in initial study are inserted in heat-transfer module to calculate the temperature and heat distribution which is labeled as *coupledstudy*.

3. Theory and Modeling

3.1. heat generation factors

Five heat generation factors have been identified in the cell and have been investigated in this simulation study [12]:

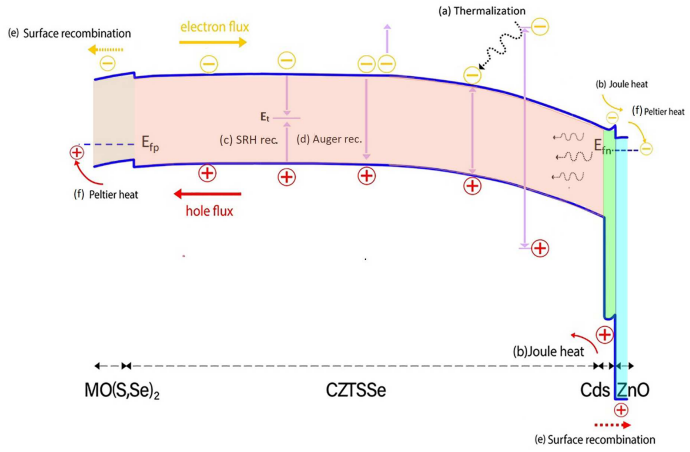

Figure 2: The five heat generation factors identified in a typical CZTSSe/CdS thin film solar cell.

1) Thermalization heat (H_{th}): generated when the hot electrons at the conduction band (generated by the hot photons (hv>E$_g$)) thermalize and step down to the edge of the conduction band due to lattice scattering.

2) Joule heat (H_{joule}): generated by carriers mobility across the cell structure under the electric field and photo-current generated and flowing across the solar cell [13].

3) Non-radiative recombination heat (H_{SRH}): generated by non-radiative recombination such as SRH recombination and Auger recombination. SRH and Auger recombination generate heat after the recombination of the electron to the mid-gap defects and the energy exchange between the carriers, respectively. Note that the direct (band-to-band) recombination does not generate heat in the cell.

4) Surface recombination (H_{surf}): recombination of the carriers at the surface traps/defects generates heat. This differs from the non-radiative recombination for it occurs at the interface and not in the bulk of the absorber layer.

5) Peltier heat ($H_{peltier}$): the heat released when electrons (holes) fall from conduction band (valance band) to quasi-Fermi level before being collected by the external circuit. The above heat generation phenomenon is described by the following equations which are also used in our simulations:

$$H_{th} = \int (hv - E_g - 3KT_{amb}).g(x,y,z,\lambda)d\lambda \quad (1)$$

$$H_{joule} = E.J_{ph} \quad where \quad E = -\nabla\phi \quad (2)$$

$$H_{SRH} = (E_g + 3KT_{amb}).(U_{SRH} + U_{Aug}) \quad (3)$$

$$H_{surf} = \int (E_g + 3KT_{amb}).U_{surf} \quad (4)$$

$$\begin{cases} H_{peltier} = H^p_{peltier} + H^p_{peltier,p} \\ H^n_{peltier} = (E_c + 1.5KT_{amb} - E_{fn}).J_{ph} \\ H^p_{peltier} = (E_{fp} - E_v + 1.5KT_{amb}).J_{ph} \end{cases} \quad (5)$$

where in Eq. (1), $g(x,y,z)$ is the photo-generation rate for every wavelength in solar spectrum and T_{amb} is the ambient temperature, E and J_{ph} are the electric field and the total photo-current in Eq. (2). $E_{c,v}$ and $E_{fn,fp}$ are the conduction and valence band and the quasi-Fermi levels for holes or electrons, respectively. U_{SRH} and U_{Aug} and U_{surf} are given by [14].

$$\begin{aligned} U_{SRH} &= \frac{np - n_i^2}{\tau_p(n + n_0) + \tau_n(p + p_0)} \\ U_{Aug} &= (C_n n + C_p p).(np - n_i^2) \\ U_{surf} &= S_n(n - n_0) + S_p(p - p_0) \end{aligned} \quad (6)$$

where n_0 and p_0 are the initial concentration of electrons and holes at equilibrium, n_i is the intrinsic carrier concentration, $C_{n,p}$ and $S_{n,p}$ are auger recombination coefficients and surface recombination velocity of electrons and holes. Note that H_{th}, H_{joule} and H_{SRH} are the volume heat components with watt/volume unit, W/m^3, whereas $H_{peltier,n}$, H_{surf} and $H_{peltier,p}$ are defined with the watt/surface unit, W/m^2 as defined for the boundary heat factors applied to the top and bottom boundaries of the cell.

3.2. heat dissipation routes

The above-mentioned mechanisms tend to heat-up the cell by increasing the "operating" temperature. However, the cell must be in thermodynamic equilibrium thus the heat is also dissipated from the cell via a couple of routes called convective and radiative cooling as given by the following equations:

$$H_{rad} = \sigma\varepsilon(T^4 - T^4_{amb}) \quad (7)$$

$$H_{con} = h(T - T_{amb}) \quad (8)$$

Where ε, σ, h, and T are the surface emissivity, Stefan Boltzmann constant, convective heat coefficient, and the *device* temperature, respectively. We set ε_{ITO}=0.2 and ε_{MO}=0.8. The other parameters values are as in Table 1 of our previous work Ref. [7].

3.3. Initial study & Coupling procedure

We followed two simulation stages to compute the electro-thermal characteristics of the cell within initial and coupled studies as defined below:
1) *initial study*: The study aimed to obtain J-V characteristics of the cell at the initial temperature of 293K. Here, the photo-generation rate (G_{tot}) is calculated by the optical module and is then inserted into the semiconductor module to calculate the initial J-V characteristics of the

cell. The temperature of the cell obtained from the heat-transfer module coupled with the semiconductor electrical module is extracted for the subsequent coupled study. 2) *coupled study*: Where the coupled modules are computed at the temperature distribution calculated from initial study.

The heat equation applies to this stage of the study as follows:

$$-k\nabla^2 T + Q = \rho_p C_p \frac{dT}{dt} \tag{9}$$

where k, C_p and ρ_d are the thermal conductivity of the material [W/(m.K)], the specific heat [J/(kg.K)], and the density at constant pressure, respectively. Q is a source term that controls the net energy absorbed across the cell. It has been assumed that the concentrated radiation was uniformly distributed on the cell surface from the air in the given cell structure.

4. Simulation Results & Discussion

The values of the parameters mentioned above have been collected in Table I of the Ref. [7]. The simulation analysis has been conducted in the following two ways:Using the optical, electrical, and thermal parameters of all layers, we simulated the Electrical and Thermal characteristics of the cell. Three heat generation factors which occur across the bulk of the cell has been plotted: H_{joule}, H_{th} and H_{SRH} for $V = V_{oc}$ and $V = 0$ V as shown in Fig. 3. Thermalization heat is the main heating source in the bulk of the CZTSSe layer especially within the depletion width at the absorber side of the CZTSSe/CdS junction. The SRH-heat is also present around the junction within the depletion width, either at V=0 or V=V_{oc} but becomes more intense within the depletion width of the CZTSSe side at open-circuited voltage. A higher H_{SRH} at $V = V_{oc}$ is because of a higher recombination rate for a higher forward bias. In contrast, the Joule heat is getting negligible at V=V_{oc} while it was comparably high at V=0. H_{joule} is directly related to built-in electric field and, therefore, at $V = V_{oc}$ the value of H_{joule} reduces to almost zero because the current-density at V_{oc} is zero (Eq. (2)). As shown in Fig. 3, H_{th}, H_{SRH} and H_{joule} are mainly at the junction and this also depends on the voltage. The practical outcome of this calculation is to develop a method to create a more reliable junction where the heat generation can be reduced from the different heating factors shown above. Finally, to get a better understanding of the total produced volume heat density within this solar cell, we have defined the next following formula, which is the sum of H_{joule}, H_{th} and H_{SRH}:

$$H_{volume} = H_{th} + H_{SRH} + H_{joule} \tag{10}$$

The 3D map of the total (volume) heat calculated using the above equation (Eq. 10) has been shown in Fig. 4a. H_{volume} has been displayed for two voltages (V= 0 and V= V_{oc}). Both 3D maps suggest that the maximum proportion of H_{volume} accumulates at the top boundary of CZTSSe layer with CdS where H_{th} is maximum. H_{joule} is zero at V= V_{oc} thus the maximum value of H_{volume} reaches to 4.3×10^9 W/m^3 whereas at V=0 the maximum of H_{volume} increases to 4.8×10^9 W/m^3 in agreement with the 2D curves presented in Fig. 3.

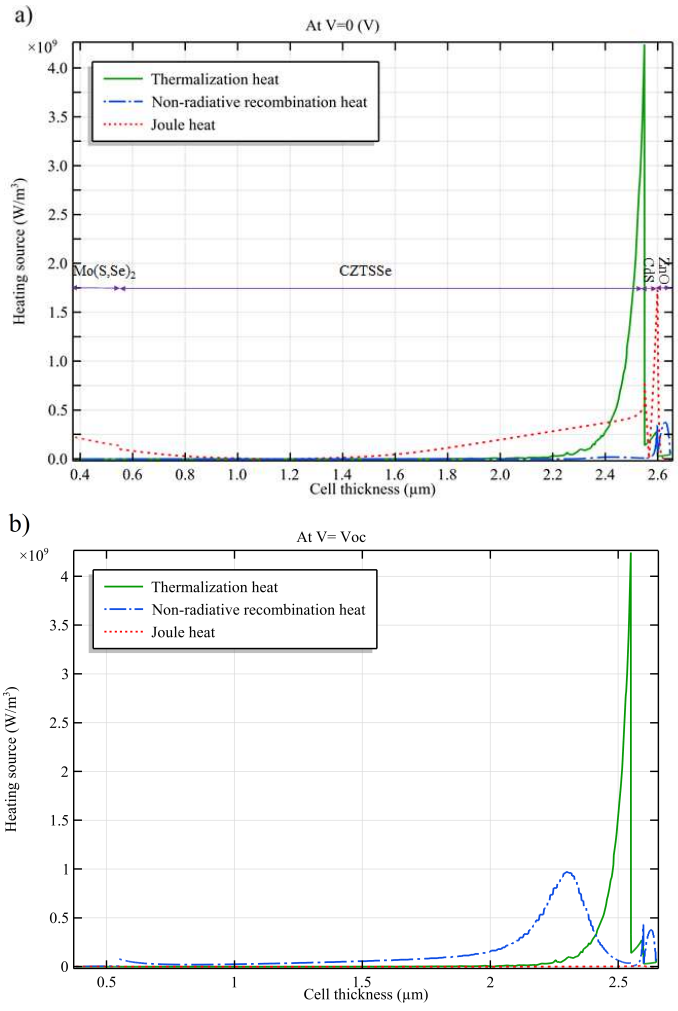

Figure 3: The profile of generated H_{joule},H_{SRH} and H_{th} across the cell at two voltages a)$V = 0$, b)V_{oc}

We have also investigated the surface recombination heat factors: H_{surf} and $H_{peltier}$. Fig. 4b displays the H_{surf} in the bottom boundary of MO/MO(S,Se)$_2$ calculated using Eq. (4 & 5). The surface recombination heat, H_{surf}, has been solely calculated for the bottom side at the metal/Mo(S,Se)$_2$ interface since the surface recombination rate at the top interface of ITO/ZnO (conductive electrodes) is negligible. Compared to the case at V=0 , H_{surf} is much higher at V=V_{oc} which is due to the increased recombination rate of the minority carriers at the interface with electrodes at V=V_{oc}. Fig. 4c maps the magnitude of heat generated by Peltier loss at the in-

terface of metal/semiconductor at V=0. $H^n_{peltier}$ is quite smaller compared to $H^p_{peltier}$ as the energy differences between the corresponding quasi-Fermi level (E_{fp}) and the valance band is smaller than the difference of (E_{fn}) and the conduction band. The practical outcome of this calculation suggests the selection of a proper metallic electrode with a high work-function to reduce the difference between the quasi-Fermi levels and the conduction/valence bands to minimize the Peltier heat generation.

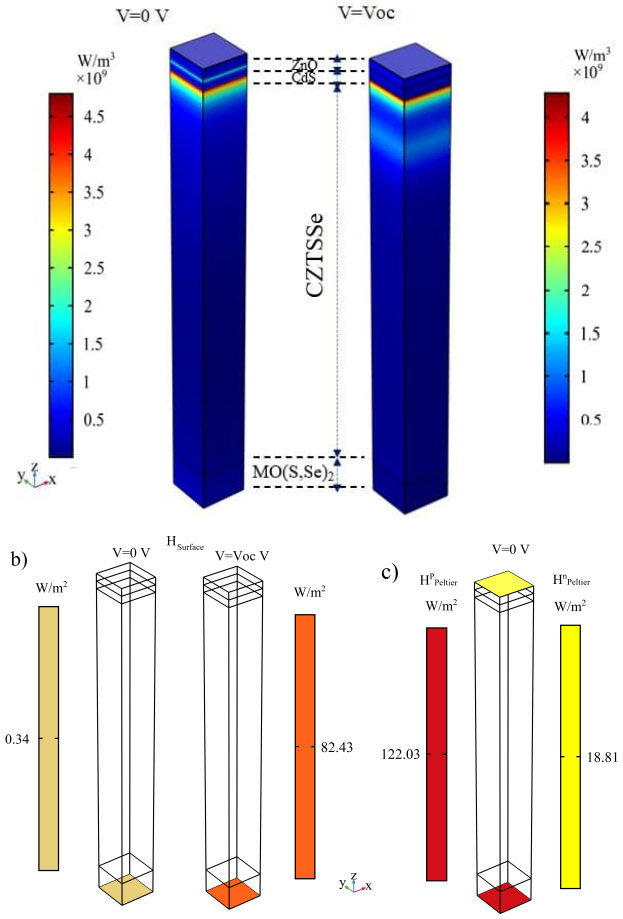

Figure 4: a)The 3D distribution map of the total volume heat generated by Thermalization, Joule and SRH recombination process (H_{volume}= H_{th}+H_{SRH}+ H_{joule}) across the bulk part of the cell. The heat at the top junction is maximum, b) the value of H_{surf} at V=0 and V=V_{oc}. Note the H_{surf} at top interface of ITO/ZnO is zero. c) $H^n_{peltier}$ and $H^p_{peltier}$ at V=0 V. The Peltier heat at V=V_{oc} is zero as there is not difference between the quasi Fermi levels and the CB/VB at this condition.

The unit of all heat components must be unified in order to compare their magnitude. Therefore H_{th}, H_{joule} and H_{SRH} are integrated (in 1D) across the length of the cell (z-axis) to convert their unit from w/m^3 to w/m^2 and are named H^{int}_{th}, H^{int}_{joule} and H^{int}_{SRH}, respectively. The integrated values and the surface heat components (H_{surf} & $H^{n,p}_{peltier}$) are displayed in Fig.5a versus voltage. The power density is mainly lost by Thermalization and Joule heating factors which are the dominant heat losses. While H_{th} is independent of voltage as given by Eq. (1), the value of H_{joule} decreases by voltage since the built-in electric field declines by approaching the V_{oc} and thus H_{joule} tends to zero. Also, power losses contributed to Peltier effects ($H^p_{peltier}, H^n_{peltier}$) are constant within 0-0.4 V and then decrease to zero at $V = V_{oc}$ where the current density is equal to zero (Eq. (5)). The power loss caused by $P^n_{Peltier}$ is higher than $P^p_{peltier}$ as the doping level of the MO(S, Se)$_2$ is lower than the ZnO layer (ZnO is more conductive). However, the H_{SRH} and $H_{surface}$ raise significantly after 0.4 V due to increased recombination at an V=V_{oc} where the Fermi level is much close to the VB/CBs and this enables more recombination of electrons and holes at the interface and within the mid-gap defects.

The total absorbed heat density in the cell (H_{abs}) is the sum of all five heat generation sources and the power density of the cell (P_{cell}) as illustrated in Fig. 5b as a function of voltage. H_{abs} is constant around 700 W/m^2 which includes the power obtained by the cell.

$$\frac{1}{A}\int \nabla.(-k\nabla T)d(x,y) = H^{int}_{th} + H^{int}_{Joule} + H^{int}_{non-rad} + H^p_{peltier} + H^n_{peltier} + H_{surface}. \quad (11)$$

It would be useful to consider the total heat generation (excluding the P_{cell}) and the trend of the heat loss by voltage. As shown in Fig. 5b, the total of five heat-generation factors are steadily declining over the voltage ranging from 0 to V_{mp} which hits the lowest-point at V_{mp} where the P_{cell} is highest. At this point, highest proportion of absorbed solar energy is converted to electrical power, and, subsequently, less thermal loss is generated. At higher voltages (for V>V_{mp}) the total-heat loss slightly rises in line with the decreasing P_{cell}. At either V=V_{oc} and V=0 a larger fraction of the absorbed energy is lost through heat generation in the cell.

4.1. Cooling & Heat Dissipation

While the heat generation increases the temperature of the solar cell, the heat dissipation tries to cool down through different cooling mechanisms. Eqs. (11 & 12) demonstrate that the total generated heat and the total dissipated heat (the left and right terms in Eq. (12)) should be equal as obliged under energy conversion law. Heat dissipation is mainly through convective cooling and radiative cooling which we also simulated in our coupled model. Total heat dissipation should be equal to total heat generation given by,

$$\frac{1}{A}\int \nabla.(-k\nabla T)d(x,y) = \frac{1}{A}\int (H_{con} + H_{rad})dA \quad (12)$$

The convective (H$_{con}$) and radiative (H$_{rad}$) cooling factors acting as the heat dissipation components have com-

puted based on equations 7 and 8 and plotted against voltage in Fig. 5b. Both cooling factors follow a similar trend as the total generated heat. Also the total heat dissipation ($H_{dissipation}$=H_{con}+H_{rad}) follows a similar trend in agreement with Eq. (12).

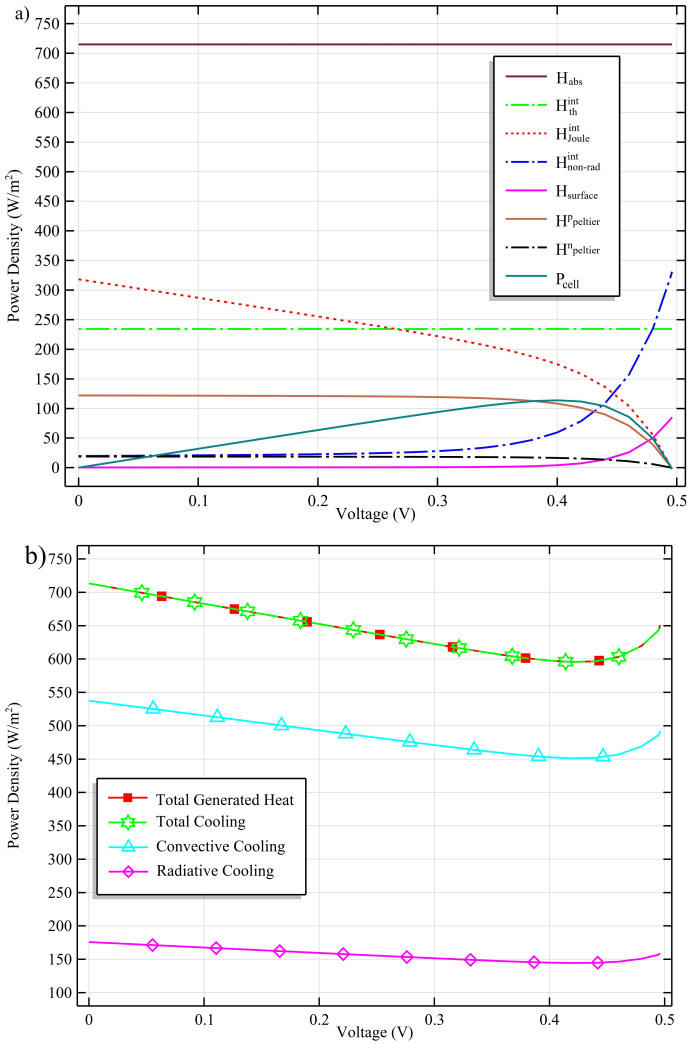

Figure 5: a) The power density of all heat generation factors (including the cell's power density (P_{cell})) versus voltage b) the total of five heat generation factors (heat loss sources), total heat dissipation (cooling), convective cooling and radiative cooling vs. voltage.

4.2. Temperature Distribution

We also investigated the temperature distribution in the structure of this solar cell to map the temperature of every layer and the whole structure in 3D format. Obviously, we expect a negligible temperature gradient in our steady-state calculations due to the thin structure of the whole device [15, 16]. As shown in Fig. 6a the temperature variation across the cell is less than 0.01K at both open-circuit and zero voltage conditions. However, the temperature is a function of voltage as presented in Fig. 6b where the temperature decreases by voltage and bottom out at 315.54 K where the system operates at its maximum power point (V= 0.46 V). At this point electrical power extracted from the cell is maximum and the energy loss via heat generation is lowest. For higher voltages, closer to V_{oc}, the temperature rises again, and the power loss via heat generation increases. Fig.6c shows the temperature profile at V= V_{mp} and the 3D map of the temperature distribution at this optimum voltage (0.46 V). Temperature is high at the top of the cell where the heat generation within the depletion width and at the junction is highest.

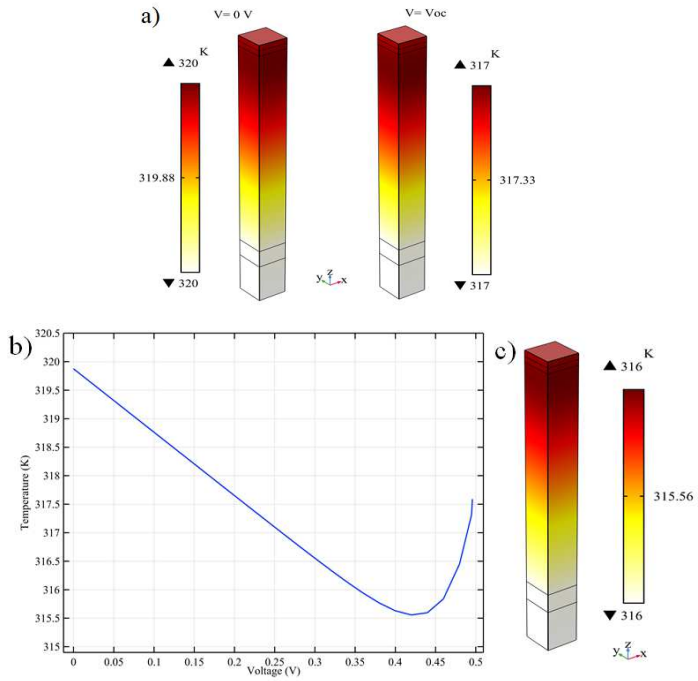

Figure 6: a) The 3D map of temperature across the cell at V=0 and V=V_{oc} where the temperature variation is less than 0.01K at both voltages, b) the temperature as a function of voltage with bottom out at 315.54 K and V=0.46 V, c) temperature distribution at the maximum power point (V=0.46 V).

4.3. Temperature impact on J-V characteristics

Finally, we study the impact of temperature on the J-V characteristics of this solar cell. Temperature can change through every heat generation factor and this can impact on J-V characteristics of the cell. This impact mainly comes from V_{oc}'s dependency on temperature (T) which is given by the following,

$$V_{oc} = \frac{kT}{q} ln \left[\frac{J_{sc}}{J_0(T)} \right] \tag{13}$$

where k is Boltzmann constant and J_0 is a dark current density, which is related to T as below:

$$J_0 = B.T^3 exp \left[-\frac{E_{g0}}{kT} \right] \tag{14}$$

where B is constant and independent of T [17]. According to the above formula, the decrease in V_{oc} at higher temperature is related to increased diode saturation current J_0 with temperature. There are some other formulas used for J_0 which are presented by a smaller power but still the relation of J_0 and T is direct and J_0 will increase at a higher temperature. Higher temperature will increase the intrinsic carrier concentration and this leads to larger rates of recombination in the cell structure [18].

Finally, we studied the change in J-V characteristics and the power-voltage curves of the cell at the temperature raised by *every* heat generation factor through coupled study and compared with the J-V of the initial study. In Fig. 7a, the J-V characteristics have been calculated for the initial temperature (T=293 K) and the coupled temperature (ranged between 315-320 K). The current-density is not affected as it is not directly temperature-dependent [19] but the V_{oc} has significantly reduced for about 0.05 V as it is a temperature-dependent parameter (as expected from Eq. (13)). The temperature distribution obtained at every voltage has been shown by the temperature bar. For the coupled study, the V_{oc} declines from 0.542 V to 0.495 V as the total temperature of the cell increases within 315 K to 320 K. Consequently, the FF value declines from 73.8% to 71.8%. A similar trend is also observed in power-density curve in Fig.7b where the voltage declines about ΔV= 0.047 V) for the temperature ranged from (315-320 K). The loss in V_{oc} and FF are in agreement with the experimental data and the simulation results presented in Ref. [20].

To achieve a deeper understanding of the impact of heat generation factors on device characteristics, we plotted the J-V characteristics at the temperature raised individually by *every* heat generation factor. Fig. 7c shows a more significant impact from H_{th} and H_{joule}, compared to other heating factors, on the performance parameters of the cell. This is in agreement with Fig. 3 and 4 where thermalization, Joule, and SRH showed maximum contribution to cell heating. On the other hand, H_{SRH}, $H_{surface}$, $H^{p}_{peltier}$ and $H^{n}_{peltier}$ (Fig. 5) show a low thermal power with minimum impact on J-V curves. All the J-V curves were calculated at the temperature raised by every heat generation factor individually while the J-V curve of the initial study was calculated at room temperature of 293 K. The J-V curve calculated at the *total* temperature raised by all heating factors (coupled study with T distribution) shows lower V_{oc}. This curve shows the impact of all heating factors on the J-V characteristics and thus is the measurable curve. The conversion efficiency of the cell decreased from 12.78% to 11.46% ($\Delta\eta$=11.11%) for the power loss due to all heat generating factors. This is in agreement with the conventional belief on detrimental impact of increased temperature on the efficiency of solar cells. However, the impact of this temperature is not as reported in many other literature [21, 22].

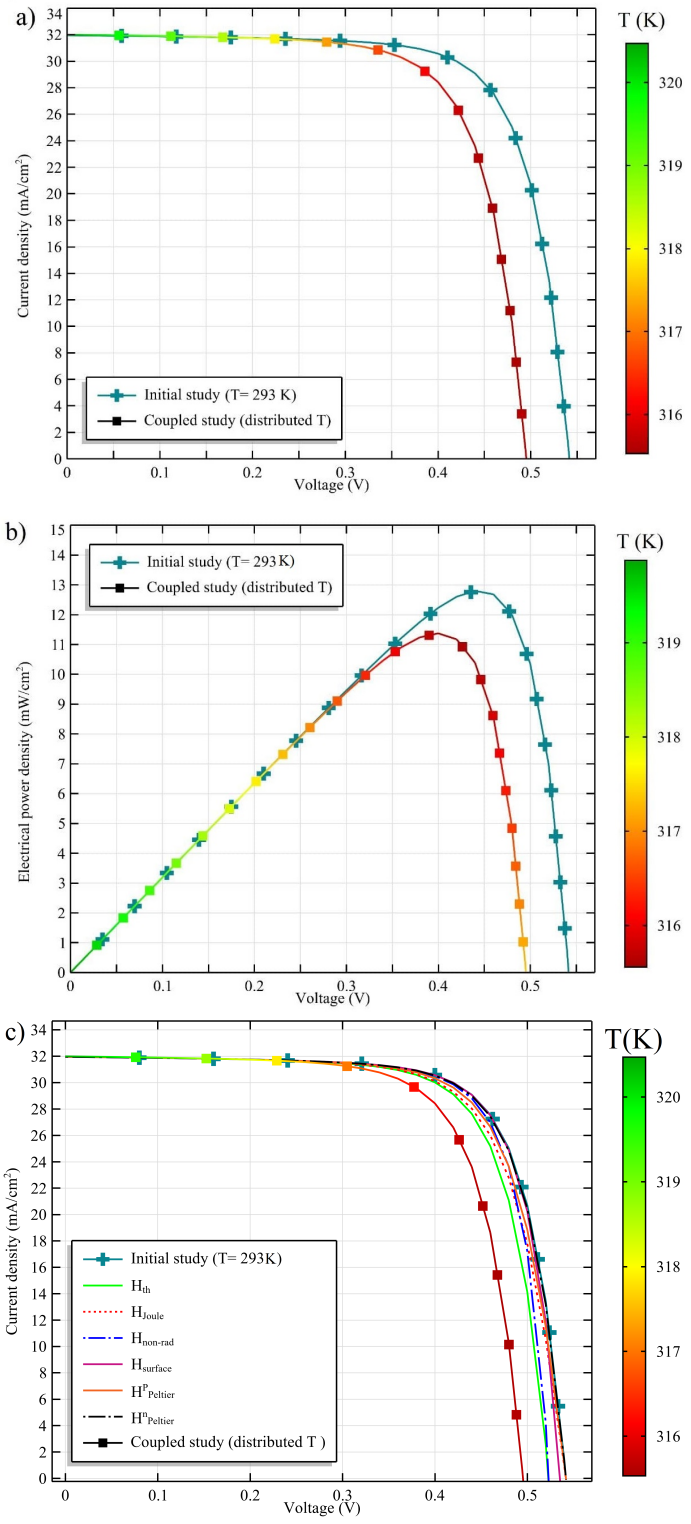

Figure 7: a) The J-V characteristics of the cell calculated at the Initial study (with T=293K), and the coupled study (for a temperature distribution within the range of 315-320 K), b) P-V curves calculated at the temperature of the initial and coupled studies. The color bar shows the calculated operating temperature at every voltage, c) the effect of each heat generation factor on J-V characteristics of the cell and the temperature raised from the total heat generating (considering all the five heat factors calculated by coupled study).

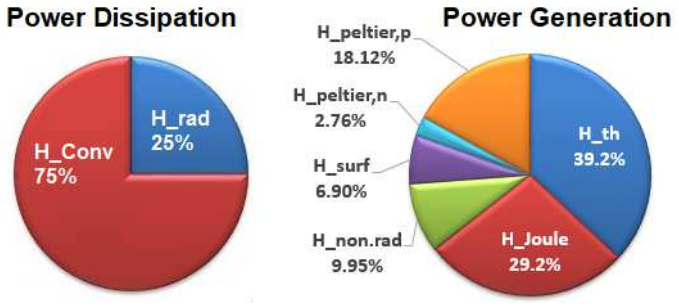

Figure 8: Heat power generation percentage through every heating factor and the contribution of cooling factors.

The J-V curves obtained from the coupled simulation is in agreement with the experimental data reported in Fig. 3c of Ref. [20] where a raise in temperature from 293K (T in our initial study) to over 320K (T in our coupled study) deterred the cell efficiency from 21.52% to 19.72%. It is also noted that although the short-circuit current density of the cell did not decrease by the heat generation in this cell, the experimental data shows that for temperatures over 320 K, J_{sc} will also experience a slight decrease due to increased J_o and from bandgap's dependency on temperature [23]. Note, in our study, the optical reflection loss and parasitic loss from the resistance of the thin layers in this solar cell structure was not calculated as was pointed in Fig. 5 of the Ref. [20] where 8% optical reflection loss and 1.6% parasitic loss was calculated.

4.4. Heat Loos Percentage

To have a better view on the power loss from the heat generation factors, we calculated the loss percentage of every heat loss component and presented by a pie chart in Fig. 8 using the power-density curves presented in Fig. 5. Note that the optical reflection loss and the parasitic resistance loss of the other layers has not been investigated in this study. Nevertheless, apart from the conversion efficiency of 12.78%, about 83.5% of the light absorption is converted to heat mainly through thermalizaiton (32.7%), Joule heating (25%) and Peltier heat (total) of 17.4%. Less heat is also generated from non-radiative recombination (SRH+Auger) 8.3% and the surface recombination heat of 0.5%. Therefore, thermalization (32.7%) and Joule heating (25%) are the main heat generators in the cell while the recombination loss from non-radiative (8.3%) and surface (0.%) are less contributing. Peltier heat is manly due to holes transition (15.14%) and a small contribution from electronc transition (2.3%). We also calculated the contribution of every heat dissipation factor. Dissipation is mainly through convective cooling (75%) and less contribution is also from radiative cooling (25%). The calculation obtained here are in agreement with the experimental evaluations presented in Fig. 3a of Ref. [24] for the power loss in thin film solar cells. This calculations help to choose a proper strategy to reduce the energy loss in solar cells by looking at the contribution of every heat generation factor individually. These results address the key heat loss sources in CZTSSe thin-film solar cells which are essential to disclose the underlying thermal degradation mechanism for performance stability and commercialization [25].

5. Conclusion

We developed FEM simulations based on coupled optical-electrical-thermal model to analyze the heat generation and dissipation across the structure of a CZTSSe/CdS thin-film solar cell (with record efficiency of12.6 %, IBM-2013). Several heat generation factors were identified at the surfaces, bulk, and the junction of the cell: thermalization heat, Joule heat, SRH-recombination heat, surface recombination heat, and the Peltier heat. Thermalization heat is highest at the junction (either at V=0 or V=V_{oc}) compared to SRH-recombination heat and Joule heating. However, when the voltage increases to V_{oc}, the SRH-recombination heat is more dominant than the Joule heating. The U_{surf} is not comparable to Peltier heat at V=0 but increases for two orders of magnitude at V=V_{oc}. Peltier heat generation behaves completely opposite way where $H_{peltier}$=0 at V=V_{oc}. Thermalization heat is dominant on current-voltage characteristics of the cell and can shift the V_{oc} for about 0.25 eV. SRH-Recombination heat has almost the same impact but can also change the fill factor too. The other heats have less impact on V_{oc}. The impact of total heat calculated from the second run (coupled study) shows about 0.0.47 V reduction in V_{oc} compared to it's *initial* value (obtained at 293K which means the heat generation deters the voltage of the cell. The heat dissipation via convective and radiative cooling has been also modeled in the balance of heat generation. The heat dissipation is mainly through convective cooling (75%) which is several times bigger than radiative cooling (25%). Finally, the coupled modeling has shown a detrimental effect of temperature increase on the power and voltage of the cell. However, the temperature depends on the voltage of the cell and reduces from V=0 towards the V_{oc}. The performance of these CZTSSe thin-film solar cells decreased by 11.11% when we considered the power loss due to all heat generating factors. Therefore, even though the temperature has not much raised than the initial value (293K), the impact on the performance is not negligible. The ΔV_{oc}=0.047 V, ΔFF= 2% has been calculated from a temperature raise from 293 to a range of 315-320 K. Therefore, the role of heat dissipation becomes an essential factor for thermal stability of thin-film solar cells.

6. acknowledgment

Authors acknowledge Dr. Isa Ahmadalidokht from the Centre for Quantum Technologies, National University of Singaporefor the the valuable discussions on developing the coupled model.

7. Conflict of Interest

Authors declare no conflict of interest.

References

[1] X. Li, Y. Zhan, C. Wang, *Prog. Photovoltaics*, 23 (2015) 628.
[2] R. Vaillon, L. Robin, C. Muresan, Ch. Menezo, *International Journal of Heat and Mass Transfer*, 49 (2006) 4454-4468.
[3] A. Shang, X. Zhai, C. Zhang, Y. Zhan, S. Wu, X. Li, *Prog. Photovoltaics*, 23 (2015) 1734.
[4] Y. An, C. Sheng and X. Li, *Nanoscale*, (2019) DOI: 10.1039/C9NR04110A.
[5] G. K. Wachutka, *IEEE Transactions on Computer-Aided Design*, 9:11 (1141).
[6] X. Li, N.P. Hylton, V. Giannini, K. Lee, N.J. Ekins-Daukes, S.A. Maier, *Prog. Photovoltaics*, 21 (2013) 109.
[7] S. Zandi, P. Saxena, M. Razaghi, N. E. Gorji, *IEEE J. of Photovoltaics*, 10:5 (2020) 1503.
[8] W. Wang, M. T. Winkler, O. Gunawan, T. Gokmen, T. K. Todorov, Y. Zhu, D. B. Mitzi, *Adv. Energy Mater.*, 4:7 (2013) 1-5.
[9] S. D. Guo, *Phys. Chem. Chem. Phys.*, 20 (2018) 7236-7242.
[10] B. Peng, H. Zhang, H. Shao, Y. Xu, X. Zhang, H. Zhu. *RSC Adv.*, 6 (2016) 5767.
[11] G. Reya, G. Larramonab, S. Bourdaisb, C. Choneb, B. Delatoucheb, A. Jacobb, G. Dennlerb, S. Siebentritta, *Solar Energy Materials & Solar Cells*, 179 (2018) 142–151.
[12] A. Shang, X. Li, *Advanced Materials*, 1603492 (2017) 1-8.
[13] S. Rampino, F. Annoni, M. Bronzoni, ..., F. Pattini, E. Gilioli, *Journal of Renewable and Sustainable Energy*, 7:1 (2015) 013112.
[14] L. Kosyachenko, *Book: Solar Cells-Thin-Film Technologies*, Intech press, 2011.
[15] Sh. Li, Ch. Wang, ..., X. Zhao, X. Li, *Nano Energy*, 78 (2020) 105378.
[16] R. Couderc, M. Amar, M. Lemiti, *IEEE Journal of Photovoltaics*, 6:5 (2016) 7508484, 1123-1131.
[17] Olivier Dupre, *PhD thesis: Physics of the thermal behavior of photovoltaic devices"*, (2016) pages: 191-195.
[18] J.A. Schwenzer, L. Rakocevic, ..., A. Quintilla, B.S. Richards, U. Lemmer, U.W. Paetzold, *ACS Appl Mater Interfaces*, 16;10(19) (2018) 16390-16399.
[19] A. Shang, Y. An, D. Ma, X. Li, *AIP Advances* 7:8 (2017) 085019.
[20] Y. An, Ch. Wang, G. Cao, X. Li, *ACS Nano*, 14 (2020) 5017-5026.
[21] S.A. Khalate, R.S. Kate, R.J. Deokate,*Solar Energy*, 169 (2018) 616-633.
[22] K.V. Sopiha, J.K. Larsen, ..., M. Edoff, Ch. Platzer-Björkman, C. Persson, J.J.S. Scragg, *J. of Materials Chemistry A*, 8 (2020) 8740-8751.
[23] A. Shang, Y. An, D. Ma and X. Li, *AIP Advances* 7 (2017) 085019.
[24] B. Lorenzi, M. Acciarri, D. Narducci, *J. of Materials Engineering & Performance*, 27 (2018) 6291-6298.
[25] L. Zhu, Y. Wang, Zh. Fang, Y. Sun, Q.Huang, *Solar Energy Materials and Solar Cells*, 94:2 (2010) 133-140.

Figures

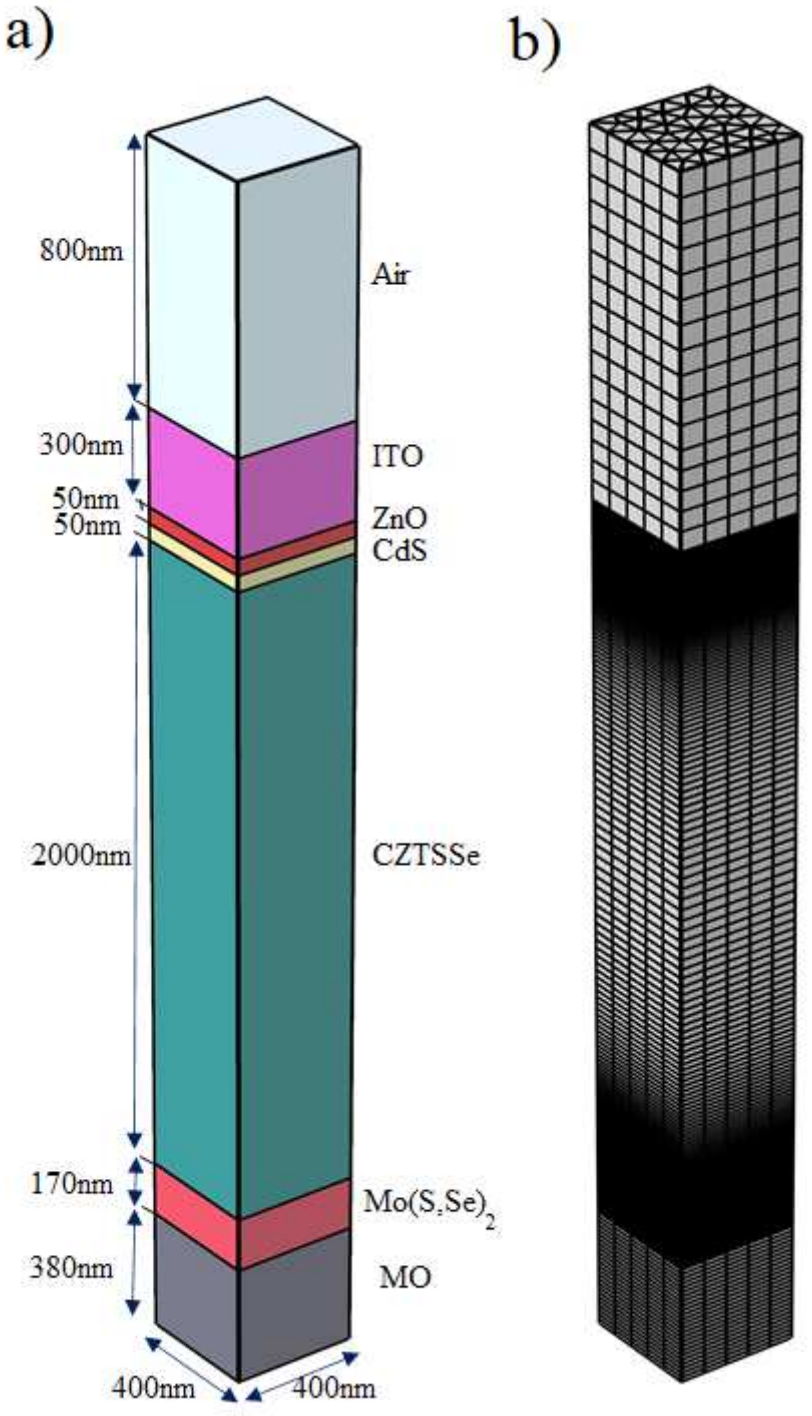

Figure 1

a)The 3D structure of the proposed CZTSSe/CdS thin film solar cell adopted from IBM's record cell efficiency [8], b) the meshed structure

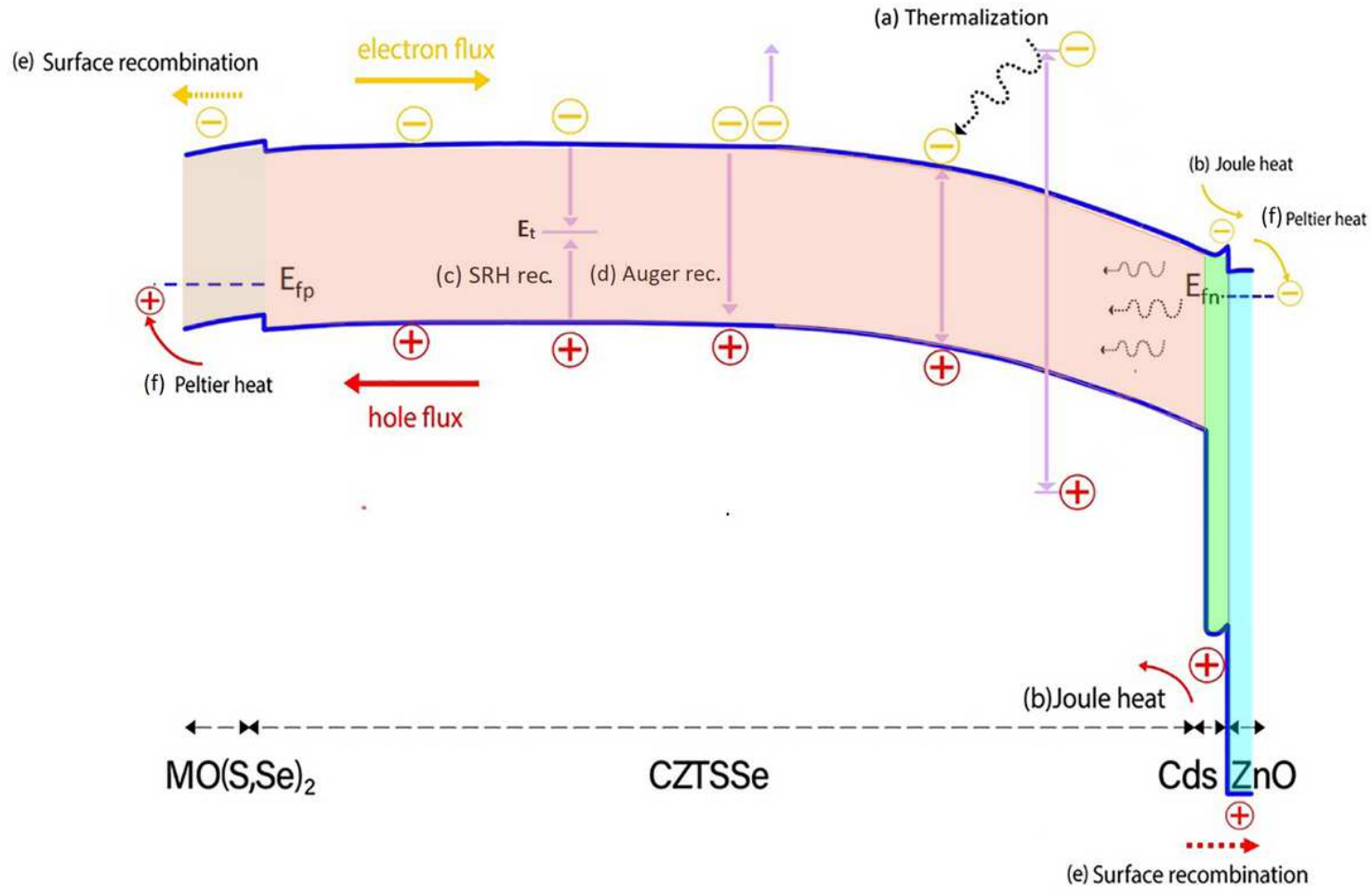

Figure 2

The five heat generation factors identified in a typical CZTSSe/CdS thin film solar cell.

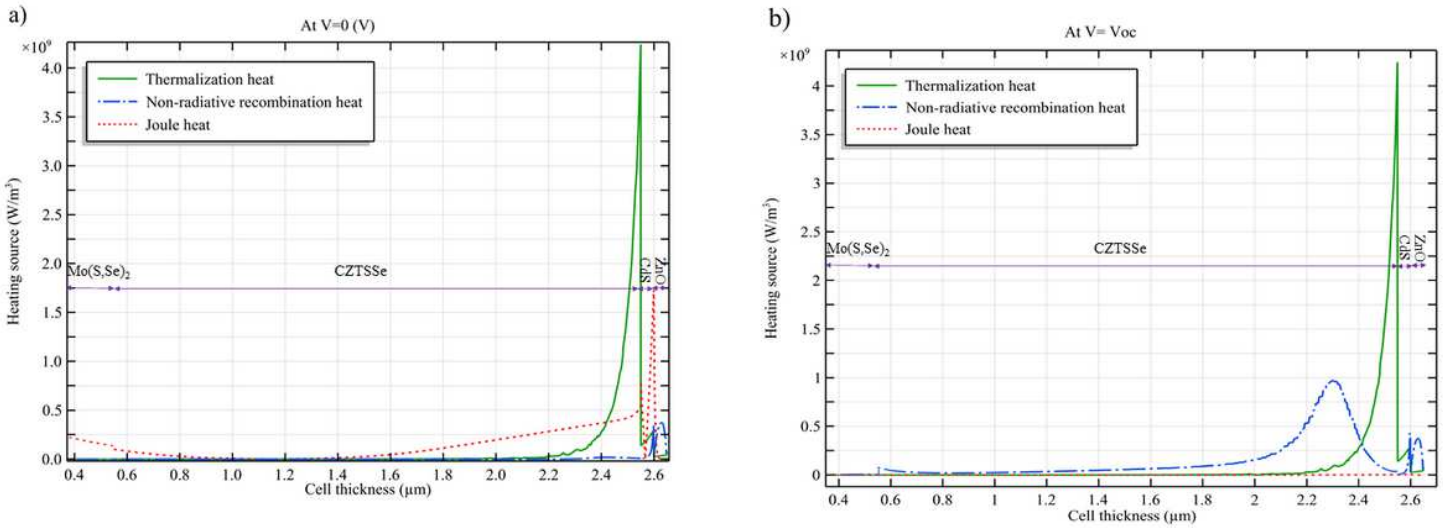

Figure 3

The profile of generated Hjoule,HSRH and Hth across the cell at two voltages a)V = 0, b)Voc

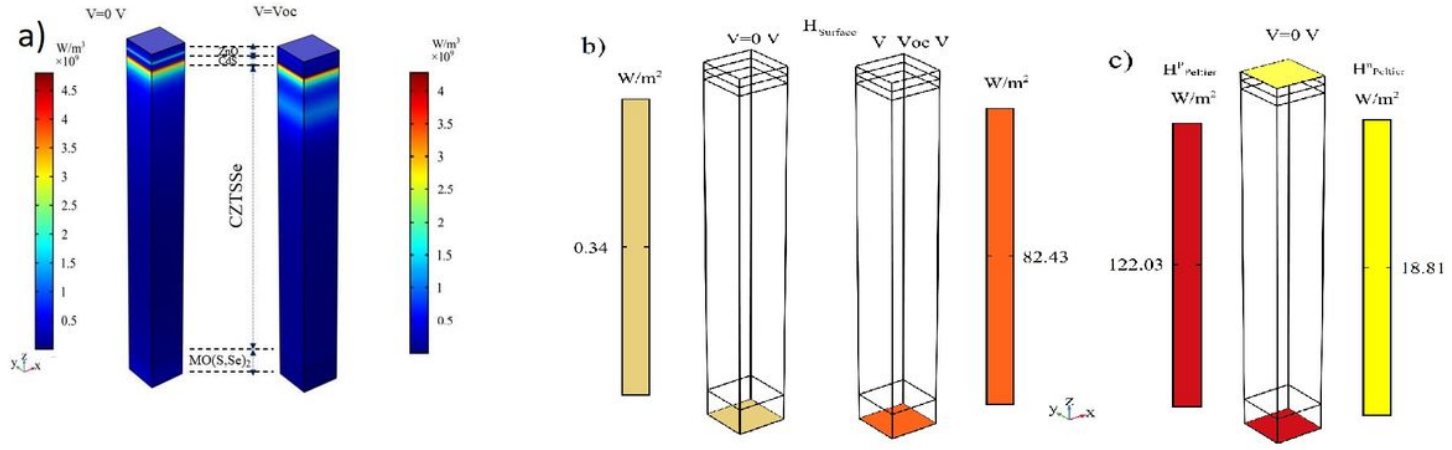

Figure 4

a)The 3D distribution map of the total volume heat generated by Thermalization, Joule and SRH recombination process (Hvolume= Hth+HSRH+ Hjoule) across the bulk part of the cell. The heat at the top junction is maximum, b) the value of Hsurf at V=0 and V=Voc. Note the Hsurf at top interface of ITO/ZnO is zero. c) Hn peltier and Hp peltier at V=0 V. The Peltier heat at V=Voc is zero as there is not difference between the quasi Fermi levels and the CB/VB at this condition.

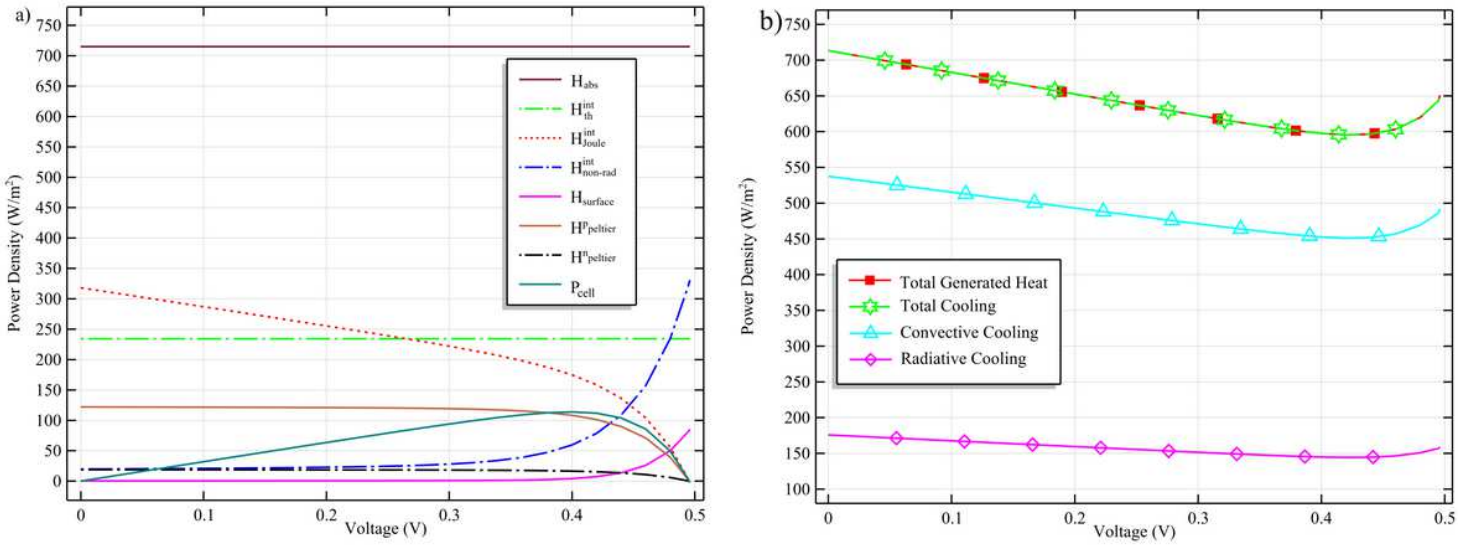

Figure 5

a) The power density of all heat generation factors (including the cell's power density (Pcell)) versus voltage b) the total of five heat generation factors (heat loss sources), total heat dissipation (cooling), convective cooling and radiative cooling vs. voltage.

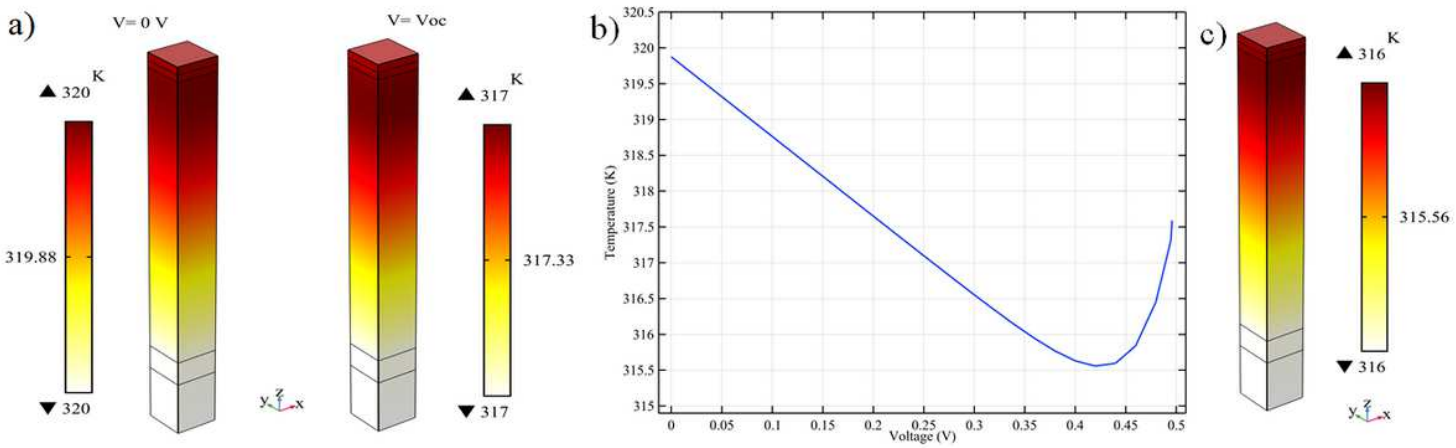

Figure 6

a) The 3D map of temperature across the cell at V=0 and V=Voc where the temperature variation is less than 0.01K at both voltages, b) the temperature as a function of voltage with bottom out at 315.54 K and V=0.46 V, c) temperature distribution at the maximum power point (V=0.46 V).

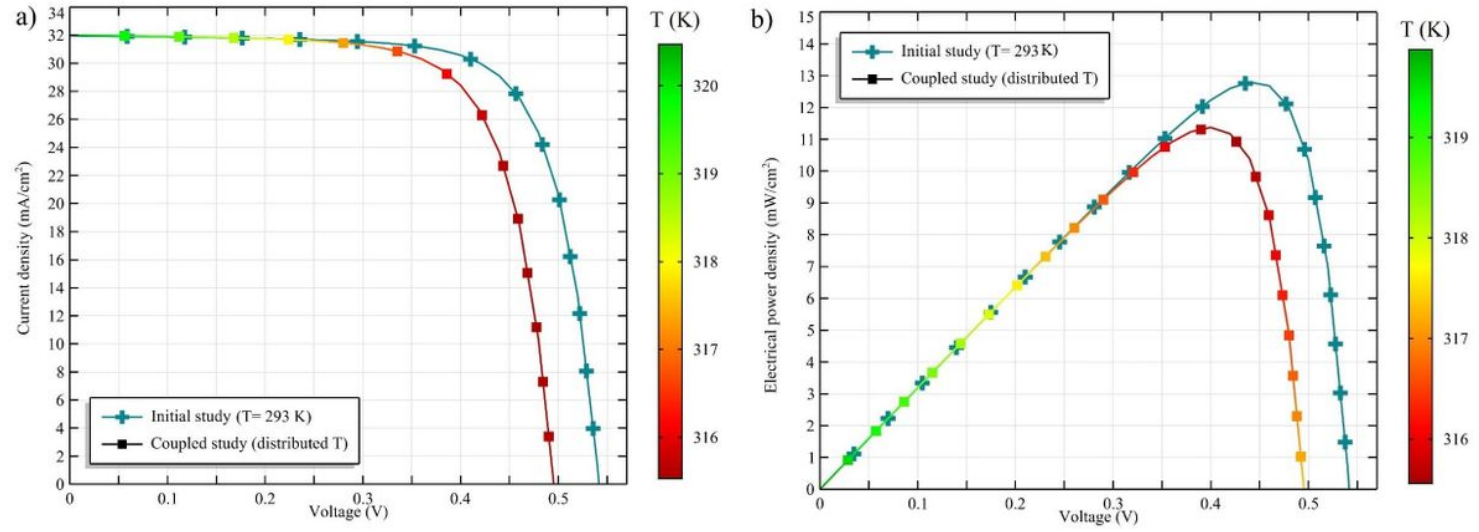

Figure 7

a) The J-V characteristics of the cell calculated at the Initial study (with T=293K), and the coupled study (for a temperature distribution within the range of 315-320 K), b) P-V curves calculated at the temperature of the initial and coupled studies. The color bar shows the calculated operating temperature at every voltage, c) the effect of each heat generation factor on J-V characteristics of the cell and the temperature raised from the total heat generating (considering all the five heat factors calculated by coupled study).

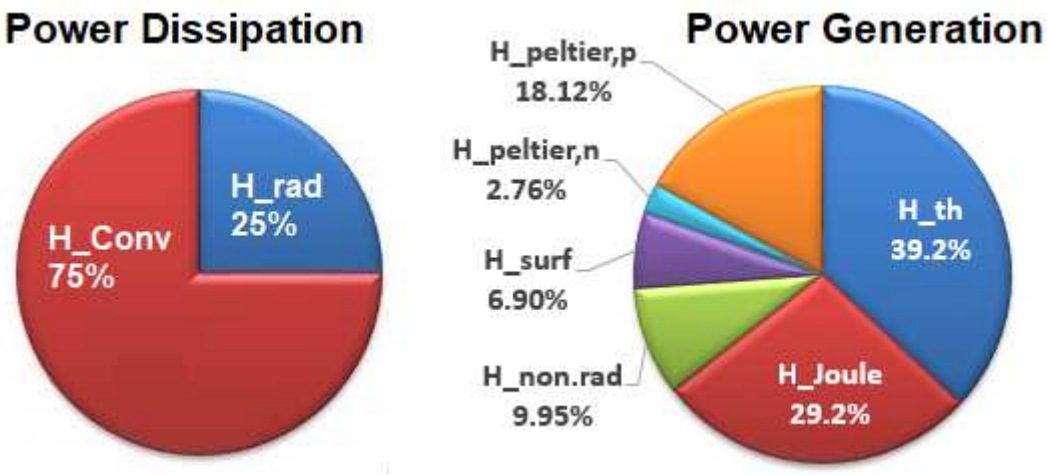

Figure 8

Heat power generation percentage through every heating factor and the contribution of cooling factors.